OPEN ACCESS

University of BRISTOL

Peer reviewed version

Link to published version (if available):
10.1039/C8CE00477C

Link to publication record in Explore Bristol Research
PDF-document

University of Bristol - Explore Bristol Research
General rights

CrystEngComm

ARTICLE

Increase of Cr solubility in cubic $Sr_2Fe_xCr_{2-x}O_{6-y}$ unit cell using sol-gel assisted synthesis and characterizations of Sr_2FeCrO_{6-y} phase

G. Song,[a] L. Bovo[b], L. R. Terry[a], O. Gómez Rojas[a,c] and S. R. Hall[a,*]

A cubic Sr_2FeCrO_{6-y} phase, for which no crystallographic data has been previously reported, was synthesized through sol-gel assisted method for the first time. EDTA and chitosan were used as chelating agents. Calcining and subsequent argon-annealing techniques were used. Analysis of the product by SQUID magnetometry showed that the material exhibited possible spin-glass transition or superparamagnetic behaviour below 50 K. The control of phase formation of the $Sr_2Fe_xCr_{2-x}O_{6-y}$ (SFCO) system has been improved and the mechanisms of phase formation were better understood. With further investigations, it is hoped that SFCO series materials will be utilized in the manufacturing of electronic devices, fuel cells and other engineering areas.

Introduction

Double perovskites ($A_2BB'O_6$) have been the focus of research in recent years, due to their unique structure, electromagnetic properties and applications.[1, 2] As an important class of double perovskite, $Sr_2FeB'O_{6-y}$ systems are particularly useful as solar cell materials and potential spintronic devices.[3-6] Due to the interactions between Fe atoms and the B' cations, oxygen deficiency and disorder in the B sites, interesting magnetic properties are often observed in this type of materials. Among this category, the $Sr_2Fe_xCr_{2-x}O_{6-y}$ (SFCO) materials have been investigated mainly theoretically,[7, 8] however few crystalline phases have been experimentally obtained and studied[9-13]. The limitations of Cr solubility in the unit cell and oxygen deficiencies create complications in phase control. The conventional method, which is solid-state synthesis, for obtaining SFCO phases cannot very well overcome these problems. To date, by manipulating the temperatures and atmosphere of reaction, three main categories of SFCO crystal phases have been obtained using the solid-state method. (i) The cubic phases $Sr_2Fe_{1.9}Cr_{0.1}O_{5.5}$ and $Sr_2Fe_{1.5}Cr_{0.5}O_5$[11, 12] are materials that can maintain the cubic structure, but contain disordered oxygen vacancies in the unit cell. The amount of Cr that could be introduced into the cubic unit cell is limited ($x > 0.75$), which is also seen in $Ca_2Fe_xCr_{2-x}O_{6-y}$ systems.[14-16] (ii) Brownmillerite (orthorhombic) phases such as $Sr_2Fe_{1.9}Cr_{0.1}O_5$ are more oxygen deficient than cubic phases, but the oxygen vacancies are more ordered.[11] (iii) Finally, the layered-rhombohedral phases (commonly referred to as 15-R) such as the $Sr_2FeCrO_{5.6}$ phase[9, 10] are the most ordered structures. Due to high level of oxygen deficiency, these crystals can no longer maintain the cubic or orthorhombic unit cell. Instead, the lattice of the 15-R structure contains Fe-rich layers and Cr-rich layers, which are stacked periodically, forming a layered-rhombohedral structure.

Average long-range magnetic order is generally observed within $Sr_2Fe_xCr_{2-x}O_{6-y}$ systems. However, the disorder of B-site cations and oxygen vacancies often cause local frustrations, impacting the overall magnetic behavior of SFCO type materials. It has been observed in general that, SFCO phases which crystallize in the 15-R and brownmillerite structures have better long-range magnetic order than the cubic structure, and contain less frustrations within the unit cell.[11-13]

The structure properties and rich magnetic behaviors in SFCO systems can be utilized in many fields of application. The varied valence states of Cr and Fe in the unit cell can improve electronic conductivity, making these materials possible fuel cell candidates. The ferro- or ferri-magnetic behaviors observed in some of the phases could be useful as magnetoresistive materials.[10] The superparamagnetic phases could be used to produce ferrofluids, which are useful in electronic devices and aerospace applications.[17, 18]

The use of chelating agents in order to fine tune the solubility of certain metals in metal oxide materials has been successfully demonstrated in systems such as Ce-Zr-La.[19] The reasoning behind this approach is to reduce reacting grain size, and increase grain number, thereby improving solubility of metal ions. In this work, we developed a sol-gel assisted synthetic method to increase the solubility of Cr in the cubic SFCO unit cell. We chose EDTA and chitosan as the chelating agents. EDTA has already been shown to be

a. School of Chemistry, University of Bristol, Bristol, BS8 1TS, UK.
b. London Centre for Nanotechnology, University College London, 17-19 Gordon Street, London WC1H 0AH, UK; Department of Innovation and Enterprise, University College London, 90 Tottenham Court Road, W1T 4TJ, London (UK).
c. Bristol Centre for Functional Nanomaterials, University of Bristol, Bristol, BS8 1FD, UK.
†Electronic Supplementary Information (ESI) available. See DOI: 10.1039/x0xx00000x

a successful chelating agent for the synthesis of high-T_c Bi-Ca-Sr-Cu-O and Y-Ba-Cu-O superconductors[20] and has been shown to be a stable chelating agent for most cations, forming a cage-like structure that effectively isolates cations from the solvent.[21] Its low cost and good chelating effect with most metal ions made it a good candidate for this method. We also used chitosan as a relatively weak, non-selective chelating agent. Its main function was to render the gel, encapsulating all metal cations in a homogeneous manner. Chitosan and EDTA could form a complex structure through dehydration, which bonds better to metal ions in weakly acidic solutions such as nitrate salt solutions.[22] Additionally the carbonisation that chitosan goes through during calcination is useful for preventing the sintering of initial phases formed at low temperatures. The gel was calcined in air and subsequently annealed in argon atmosphere. A cubic SFCO phase with nominally equal amounts of Fe and Cr was observed, and further investigated.

Experimental

Synthesis

Sol-gel preparation: Starting materials were $Sr(NO_3)_2$, $Cr(NO_3)_3 \cdot 9H_2O$ and $Fe(NO_3)_3 \cdot 9H_2O$. The synthesis was carried out using a 2/1/1 Sr/Fe/Cr stoichiometry, targeting the Sr_2FeCrO_{6-y} composition. EDTA was added following 1/1/2 Fe/Cr/EDTA stoichiometry. The nitrates (0.2 mmol Sr, 0.1 mmol Fe, 0.1 mmol Cr) were first dissolved in 5 μL deionized water, to which 0.2 mmol EDTA and 0.04 g chitosan (medium molecular weight) were added. The mixture was stirred to make a paste and heated at 80 °C on a hotplate for ~2 h to make the excessive water evaporate. The resulting mixture was a smooth purple gel.

Sol-gel synthesis route: The sol-gel mixture was then calcined in a furnace (Carbolite) in air atmosphere at 1100 °C for 24 h, the heating rate was set at 5 °C/min. The product was then ground, and moved to a tube furnace (Carbolite) where it was annealed under flowing argon for an additional 18 h at 1100 °C, the heating rate was also 5 °C/min. For clarity, the pre-argon anneal material will be referred to as Sol-Air, and the post-argon anneal material as Sol-Argon.

Solid-state route: Starting materials (stoichiometric) $SrCO_3$, Cr_2O_3 and Fe_2O_3 were thoroughly mixed and pressed into a pellet. The pellet was then calcined and subsequently annealed with the same conditions as those used in the sol-gel assisted route. For clarity, the samples pre- and post- anneal are referred to as SS-Air and SS-Argon.

Study of temperature: Solid-state and sol-gel starting materials were prepared using aforementioned methods. These were respectively heated to temperatures between 300 – 1100 °C (step size 100 °C) in air atmosphere in a furnace (Carbolite). Heating rate was 5 °C/min, and the dwell time was limited to 1 h.

Study of dwell time: Solid-state and sol-gel starting materials were prepared using aforementioned methods. These were respectively heated to 1100 °C in air atmosphere in a furnace (Carbolite). Heating rate was 5 °C/min. The samples were then maintained at 1100 °C for 1 h, 2 h, 6 h, 12 h and 24 h, before being cooled down to room temperature with an approximate 5 °C/min rate.

Characterisation method and equipment

The crystal structures of all products were determined via powder X-ray diffraction (XRD; Bruker D8), with CuKα radiation (λ=0.154 nm). Transmission electron microscopy (TEM; JEOL 1400) with selected area electron diffraction (SAED; JEOL 1400) was used to examine morphology and crystal structure of particles, operating at 120 kV. Scanning electron microscopy and EDX (SEM; JEOL IT300) was used to determine the surface morphology and elemental content of the material. XRD patterns were indexed according to information held in the International Centre for Diffraction Data (ICDD) databases. Rietveld analysis was performed using the Profex 3.9.2 GUI, which runs the BGMN Rietveld program. The magnetic properties of the materials were characterised using SQUID magnetometry; an applied magnetic field of 50 Oe was used and magnetization was measured in the temperature range of 4-300 K. Zero-field cool (ZFC, where the sample is first cooled without an applied field, and then susceptibility is measured while warming up) and field cool (FC, where the sample is first cooled under an applied field, and then susceptibility is measured while warming up) modes of measurement were used.

Results and discussions

Crystallography of Sol-Air and Sol-Argon samples

The XRD data of Sol-Air and Sol-Ar samples are presented in Figure 1. Sol-Air contained the cubic perovskite phase $Sr_2Fe_{1.6}Cr_{0.4}O_5$ unit cell and secondary phase $SrCrO_4$ (Figure 1-a). Reflections at d=3.92, 2.77, 2.26, 1.96, 1.60, 1.39, 1.24 Å belong to the cubic phase, corresponding with the reflection planes (100), (110), (111), (200), (211), (220), (310) respectively. Reflections at d=3.700, 3.452, 3.260, 3.128, 3.001, 2.545, 2.236, 2.062, 1.833, 1.407 Å correspond to the planes (020), (200), (120), (210), ($\bar{1}$12), ($\bar{2}$12), ($\bar{3}$11), (212), (132) and (124) of the $SrCrO_4$ phase. The XRD pattern of Sol-Argon (Figure 1-b) appeared to resemble a typical vacancy disordered cubic perovskite phase that has been previously reported in the SFCO system, but the peaks are noticeably broader. A similar cubic pattern with broadened lines was observed by Gibb et al., attributed to the phase $Sr_2FeCrO_{5.51}$.[9, 23] However, to the best of the author's knowledge, the exact crystallographic data for $Sr_2FeCrO_{5.51}$ was not reported. Via EDX analysis (Figure S5, S6), the chemical composition of the Sol-Air and Sol-Argon samples were determined. The results indicated the Fe-Cr content ratio maintained 1:1 pre- and post-anneal. The usual
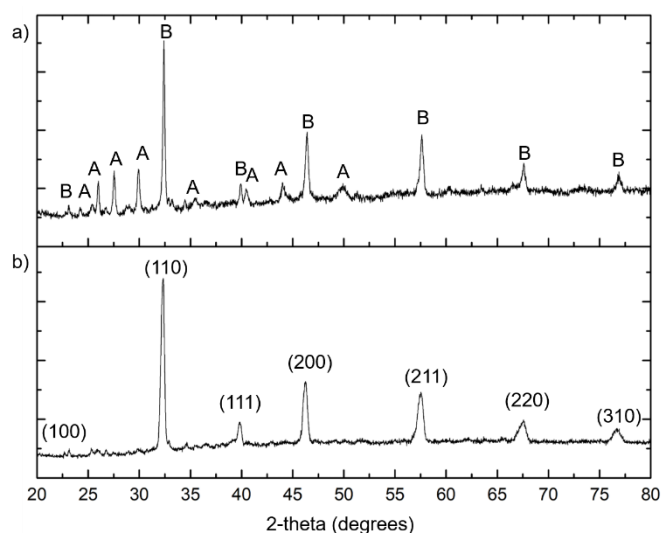
Figure 1 Powder XRD: a) XRD of Sol-Air. A=$SrCrO_4$, B=$Sr_2Fe_{1.6}Cr_{0.4}O_5$; b) XRD of Sol-Argon, indexed as $Pm\bar{3}m$ structure

the main component. Most likely, this happened because the annealing process did not affect the material in the pellet uniformly, and certain parts of it became more oxygen deficient, forming the 15-R phase. As discussed in the next section, by improving homogeneity of reactants, the 15-R phase can be inhibited from forming. While not within the scope of this paper, it is possible that better chelating systems than the EDTA-chitosan system will be found, and that we will eventually be able to remove the 15-R phase entirely from the final product. The solid-state synthesis products were examined using XRD (Figure S7). Rietveld analysis was performed (Figure S10, S11). SS-Air (Figure S10) contained 26.15% $SrCrO_4$, 4.95% $SrCO_3$, 23.12% $Sr_2Fe_{1.6}Cr_{0.4}O_5$ (cubic) and 45.77% $Sr_2FeCrO_{5.6}$ (15-R). SS-Argon (Figure S11) contained 15.88% $SrCrO_4$, 2.44% $SrCO_3$, 2% $Sr_2Fe_{1.93}Cr_{0.07}O_5$ (orthorhombic), 16.1% $Sr_2Fe_{1.6}Cr_{0.4}O_5$ (cubic) and 63.6% $Sr_2FeCrO_{5.6}$ (15-R).

Comparing the results, the most notable difference was that much more 15-R phase were formed in the solid-state synthesis route compared to the sol-gel route, during both the calcination and the annealing steps. There was almost no 15-R phase forming in the Sol-
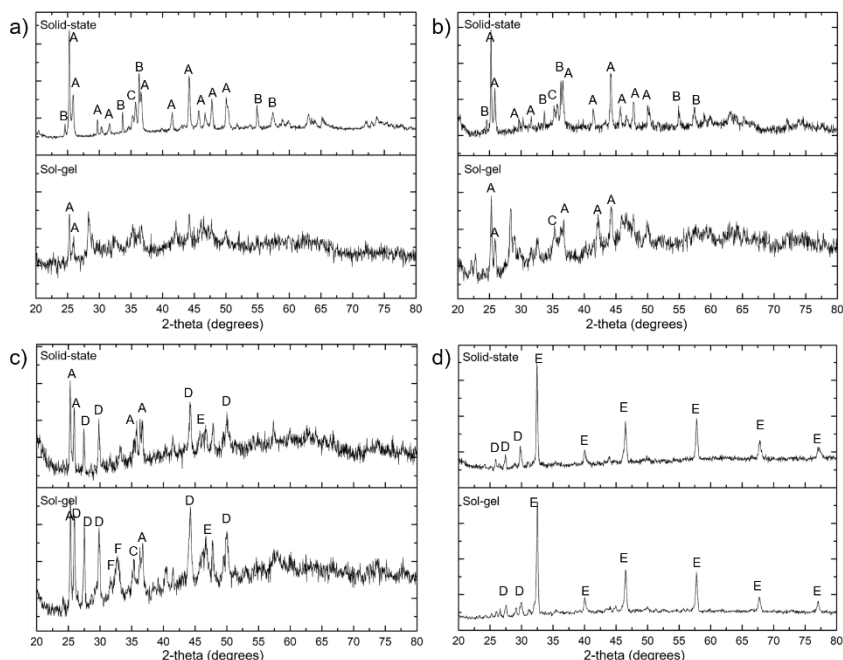

Figure 2 XRD patterns of solid-state and sol-gel samples at different temperatures of calcination: a) calcination at 300 °C; b) calcination at 500 °C; c) calcination at 700 °C; d) calcination at 1100 °C. Phases: A=$SrCO_3$; B=Cr_2O_3; C=Fe_2O_3; D=$SrCrO_4$; E=$Sr_2Fe_xCr_{2-x}O_{6-y}$ (0.8<x<1); F=$Sr_2Fe_2O_5$

limitations to Cr solubility in the cubic unit cell[9, 11, 12] does not seem to apply to the results shown here.

Rietveld analysis was used to calculate the phase composition of Sol-Air (Figure S8). The material mainly contained $SrCrO_4$ and $Sr_2Fe_{1.6}Cr_{0.4}O_5$ (cubic), with also trace amount of $Sr_2FeCrO_{5.6}$ (15-R). To account for the disorders in the cubic structure unit cell observed in Sol-Argon, we used the existing XRD pattern of $Sr_2Fe_{1.9}Cr_{0.1}O_{5.5}$ as the structure model of a vacancy disordered cubic perovskite for the calculations. Rietveld analysis on Sol-Argon (Figure S9) show that the phase contained 23.3% 15-R phase, and 67.5% vacancy disordered cubic phase. The lattice constant of the cubic phase was a=3.93 Å, which was larger than that of $Sr_2Fe_{1.9}Cr_{0.1}O_{5.5}$ (a=3.88 Å). The calculations suggest that the Sol-Air material reacted to form two different phases during argon annealing, with the cubic phase being

Air sample, however it was the main composition of the SS-Air sample. Similarly, the 15-R phase was not the dominant phase in the Sol-Argon sample, but was so in the SS-Argon sample.

To further understand the difference in the two reaction routes, we studied the phase formation at different temperatures and using different dwell times.

Comparisons in the reaction mechanism of sol-gel route and solid-state route

Temperature study: A study of phase formation between 300 – 1100 °C was conducted using methods described in the Experimental section. XRD was used to analyze the resulting samples. The full
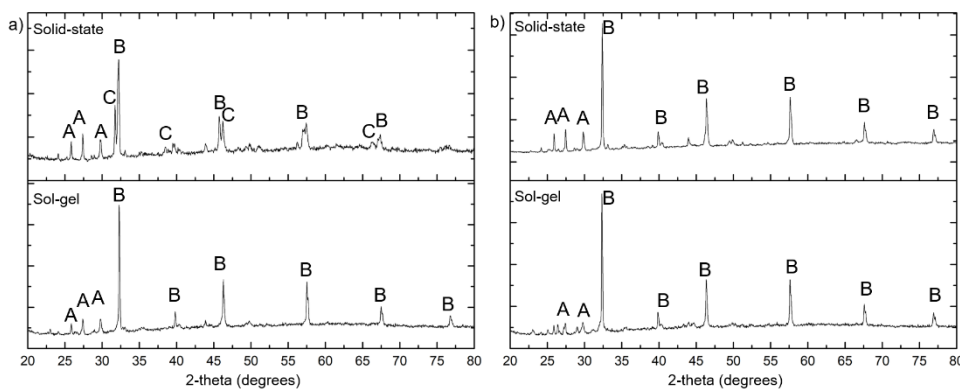
Figure 3 XRD patterns of solid-state and sol-gel samples calcined at 1100 °C, with different dwell times: a) dwell time 24 h; b) dwell time 2 h. Phases: A= $SrCrO_4$; B= $Sr_2Fe_xCr_{2-x}O_{6-y}$ (0.8<x<1); C= possible 15-R $Sr_2Fe_xCr_{2-x}O_{6-y}$ phase

results are given in the ESI (Figure S1, S2). The discussions focus mainly on the patterns given in Figure 2.

In the sol-gel samples, crystal phases are clearly not well formed at lower temperatures (Figure 2-a, b, Figure S1). Only the $SrCO_3$ phase can be clearly identified below 500 °C, which was formed due to carbonization of the Sr ions during dehydration. There were also possible formation of the phases FeO and $Sr_2Fe_2O_5$, but these phases did not become dominant in the sample. From 700 - 900 °C, $SrCrO_4$ content and $Sr_2Fe_xCr_{2-x}O_{6-y}$ content increase, while $SrCO_3$ begin to decrease. By 900 °C $SrCO_3$ is no longer visible in the diffraction pattern. From 900 – 1100 °C, the peak at $2\theta \approx 32.5$ ° is seen to shift to lower angles, with the corresponding d spacing value increasing from 2.726 Å (900 °C) to 2.757 Å (1100 °C). This temperature range also saw the decline of $SrCrO_4$ content (though not eliminated), which is because the $SrCrO_4$ phase partly reacts with the $Sr_2Fe_xCr_{2-x}O_{6-y}$ unit cell in this temperature range.[9, 15] The shift of peak shows the $Sr_2Fe_xCr_{2-x}O_{6-y}$ phase unit cell expanded due to incorporation of Cr. In the solid-state sample meanwhile, we observed a breakdown of the starting material phases from 300 through 700 °C. The main final phases $SrCrO_4$ and $Sr_2Fe_xCr_{2-x}O_{6-y}$ could be clearly seen at 700 °C. At high temperatures the similar shift of peaks was seen. Unlike in the sol-gel route, phase composition was relatively simple in the solid-state route. Instead of the sol-gel route having multiple competing phases at the lower temperatures, which then eventually formed the final phases, the solid-state route reaction was simply from the starting materials to the final $SrCrO_4$ and $Sr_2Fe_xCr_{2-x}O_{6-y}$ phases.

Dwell time study: The effect of calcination dwell time on the formation of phases was studied, following the procedures described in the Experiment section. The full results are given in the ESI (Figure S3, S4). The discussions focus mainly on the patterns given in Figure 3. As can be seen, in both cases crystalline phases were well established after 2 h of calcination. The phase component was also consistent during most of the calcination process.

Interestingly, while the phase components in the sol-gel sample remained roughly consistent throughout the study, the components in the solid-state sample saw a significant transition at the 24 h point. Shown in the XRD pattern, the single peak at 32° became a double peak, which is characteristic a decrease in the symmetry of the unit cell. This asymmetry may be caused by the formation of oxygen vacancies within the unit cell, which is due to high temperature and long dwell time. The overall pattern indicated that the material was going through phase transition from the cubic structure to the final 15-R structure.

This shows that at 1100 °C, the dwell time of the solid-state calcination did not affect the reaction linearly. This result suggests that when dwell time was long enough, it is thermodynamically preferable for the $Sr_2Fe_xCr_{2-x}O_{6-y}$ phase to transform into the 15-R structure. However, this phase transition was not observed in the sol-gel route, at least not by the 24 h mark, which indicates that in the sol-gel route, this phase transition process could be delayed.

The differences of the results reflect the difference in mass transport efficiency between the sol-gel assisted method and the solid-state method. The results indicate that the 15-R phase was a preferable phase for the solid-state synthetic route, but was inhibited from forming in the sol-gel route. We speculate that the cubic Sr_2FeCrO_{6-y} phase should be treated as an intermediate phase. The study of dwell time seemed to show that loss of oxygen in the unit cell, due to prolonged heating or increased temperature, will cause this phase to ultimately transition to the 15-R phase. However, the formation of this phase is a fast reaction compared to the formation of the 15-R phase, meaning that it could be obtained through very careful control of the reaction system. For this reason, the use of the sol-gel as a starting material was crucial to obtaining this cubic phase. The calcination of a sol-gel rather than solid mixture would create a higher number of reacting grains and therefore more grain boundaries, while also reducing the grain size to nanoscale. This meant higher ion transporting efficiency, particularly for more Cr ions to be dissolved into the $Sr_2Fe_xCr_{2-x}O_{6-y}$ unit cell. This became apparent in the argon annealing step, when a high percentage of Cr was able to dissolve in the cubic unit cell. Moreover, the metal ions were thoroughly randomised due to the use of non-specific chelating agents, forming a homogeneous gel as the starting point of the reaction. In contrast, ions in the solid-state process were restrained within the crystal structures of the starting materials. This restricts the efficiency of ionic diffusion during the calcination process and resulted in the formation of 15-R phase. It is apparent from the results that this randomising of the reactants was helpful in inhibiting the formation of 15-R phase early in the calcination stage, and forming the cubic Sr_2FeCrO_{6-y} phase during annealing. Finally, in the
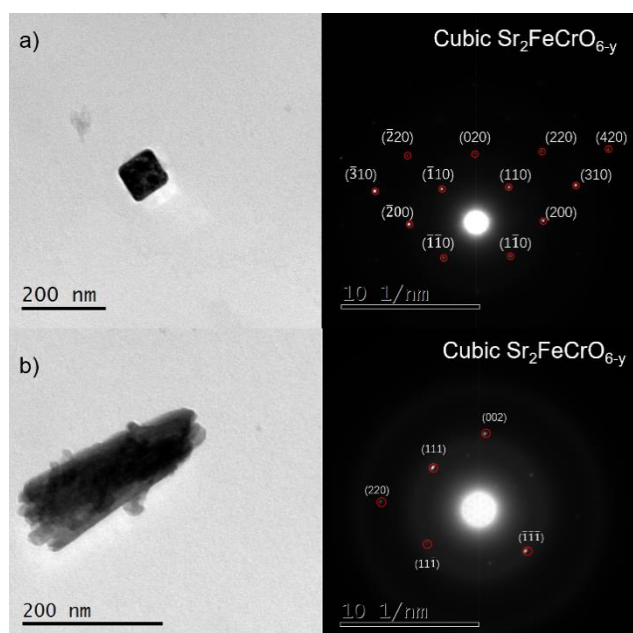
Figure 4 Electron diffraction patterns of particles in the Sol-Argon sample: a) cubic shaped single crystal particle, indexed as a cubic phase; b) crystallite, indexed as a cubic phase
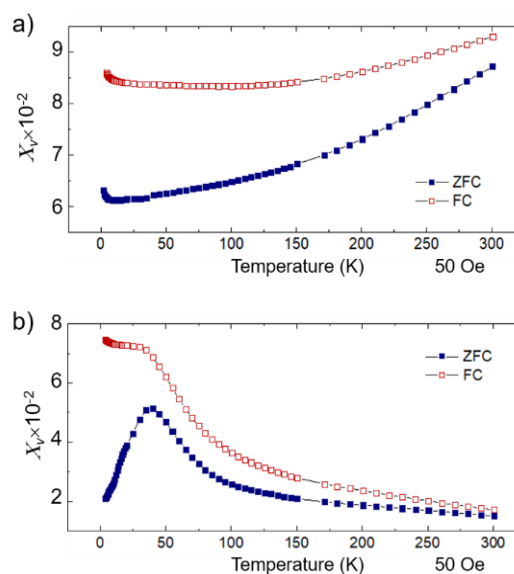

Figure 5 M-T measurements (ZFC and FC modes, 4-300 K): a) M-T curve of Sol-Air; b) M-T curve of Sol-Argon. X_v represents volume magnetic susceptibility.

calcination of the sol-gel, carbonisation of the organic materials and the cocooning of the emergent crystalline phases are important processes which lead to the formation nanoscopic intermediate species. This process leads to the crystallisation of $SrCrO_4$ and $Sr_2Fe_{1.6}Cr_{0.4}O_5$ phases in a homogeneous manner, which improved ionic diffusion between reactants during the annealing step. This feature of non-specific chelation to aid synthesis has also been seen to work effectively with the phase control of other types of oxides, such as our work on $SrNbO_x$ materials.[24]

Characterisation of morphology

The macroscopic morphology of Sol-Air and Sol-Argon was examined via SEM and TEM (Figure S12). The outgassing of the organic chelating agents as calcination progressed formed sponge-like structures (Figure S12-a). TEM image of Sol-Air (Figure S12-e) showed that the particles were 100-500 nm in size. TEM image of Sol-Argon sample (Figure S12-c, f) showed a cluster type morphology, representing the diffusion of particles during annealing. The size of the cluster is >1 µm. Direct evidence of organic cocooning of crystalline phases was observed by examining the particles of sol-gel samples at lower temperatures (Figure S12-g, h).

The Sol-Argon sample was further examined by electron diffraction. Cubic Sr_2FeCrO_{6-y} single crystal particles (Figure 4-a, b) can be observed, with clear electron diffraction patterns. This type of particles was generally small, around 50-500 nm in size. A 15-R phase particle (Figure S12-c, d) was also observed under electron diffraction. This particle was much larger, >1 µm in size, and appeared to be a cluster of smaller grains. The observed phases provide further support for the XRD analysis, and the formation of a cubic Sr_2FeCrO_{6-y} phase.

Analysis of magnetic properties

Using SQUID magnetometry, we measured the magnetic susceptibility of Sol-Air and Sol-Argon against temperature. The temperature range was 4-300 K. Sol-Air (Figure 5-a) showed positive magnetic susceptibility, but the curve did not fit that of paramagnetic behavior. The trend of the curve suggests that the material has a magnetic ordering temperature above 300 K, and is attributed to the behaviour of $Sr_2Fe_{1.6}Cr_{0.4}O_5$, which is the main composition of Sol-Air, and antiferromagnetically orders at $T_N \sim 565$ K.[12] Since the susceptibility of the main secondary phase $SrCrO_4$ is very weak (-5.1×10^{-6} cm^3/mol)[25] we can disregard its contribution to the overall susceptibility measurement of Sol-Air. In Sol-Argon (Figure 5-b) a divergence between the FC and ZFC curves is seen at around 40 K. This type of divergence is usually due to superparamagnetic behaviour or spin-glass transition. The divergence between FC and ZFC curves still existed up to 300 K. This feature has also been observed in the cubic phase $Sr_2Fe_{1.9}Cr_{0.1}O_{5.5}$ at ~60 K.[11] We speculate that, like the vacancy disordered cubic $Sr_2Fe_{1.9}Co_{0.1}O_{5.5}$, this divergence was caused by oxygen vacancy disorders within the unit cell. While beyond the scope of this communication, we believe further investigations such as neutron diffraction will be helpful in clarifying the crystal structure parameters of this sample.

Conclusions

An oxygen-vacancy disordered cubic phase Sr_2FeCrO_{6-y}, containing high Cr content was observed, which has not been reported to-date. While the general belief is that cubic Sr_2FeCrO_{6-y} cannot be synthesized due to the limitations on Cr solubility, we present a possible route to increase its solubility using sol-gel assistance. The key difference between a simple solid-state reaction, and the use of the sol-gel route, is that the sol-gel could afford a fully randomized environment for the initial ions to react. Moreover, during the calcination process, the formation of cocooning structures and the

ARTICLE   Journal Name

carbonization process was crucial to restraining the particle growth to nanoscale, and thus maintaining reactivity of the particles throughout the calcination process. In contrast, solid-state calcination processes tend to be accompanied by the sintering of initially formed phases at lower temperatures, which reduces the reactivity of reactants. The results show that the sol-gel route could effectively delay the formation of the 15-R phase, leading instead to the formation of cubic Sr_2FeCrO_{6-y}.

The formation of this phase demonstrated the possibility of obtaining new SFCO phases not yet reported. This phase shows interesting magnetic properties and is speculated to have localized disorder of oxygen vacancies. Its structural properties can be utilized in fuel cells. The speculated superparamagnetic properties this phase exhibits shall be further investigated. Potential applications in aerospace engineering and the manufacturing of electronic devices can be expected from this type of material. We have shown in this paper that by creating a homogeneous and non-specific chelating system as the starting material, better control over phase formation was achieved. Certainly, the proposed combination of EDTA and chitosan is not necessarily the most effective, and further work is being done to test the effectiveness of other chelating agents such as DTPA, and ionic liquid solvent systems. It is hoped that using sol-gel techniques, and combining different chelating agents, it will be possible to control the crystallization of complex systems like the SFCO system.

Conflicts of interest

There are no conflicts to declare.

Acknowledgements

Notes and references

1. J. Androulakis, N. Katsarakis, J. Giapintzakis, N. Vouroutzis, E. Pavlidou, K. Chrissafis, E. Polychroniadis and V. Perdikatsis, *Journal of Solid State Chemistry*, 2003, **173**, 350-354.
2. M. T. Anderson, K. B. Greenwood, G. A. Taylor and K. R. Poeppelmeier, *Progress in Solid State Chemistry*, 1993, **22**, 197-233.
3. L. Ortega-San Martin, J. P. Chapman, L. Lezama, J. J. S. Garitaonandia, J. S. Marcos, J. Rodríguez-Fernández, M. I. Arriortua and T. Rojo, *Journal of Materials Chemistry*, 2006, **16**, 66-76.
4. R. Pradheesh, H. S. Nair, C. Kumar, J. Lamsal, R. Nirmala, P. Santhosh, W. Yelon, S. Malik, V. Sankaranarayanan and K. Sethupathi, *Journal of Applied Physics*, 2012, **111**, 053905.
5. T. Shimada, J. Nakamura, T. Motohashi, H. Yamauchi and M. Karppinen, *Chemistry of Materials*, 2003, **15**, 4494-4497.
6. M. Besse, V. Cros, A. Barthélémy, H. Jaffrès, J. Vogel, F. Petroff, A. Mirone, A. Tagliaferri, P. Bencok and P. Decorse, *EPL (Europhysics Letters)*, 2002, **60**, 608.
7. K.-W. Lee and K.-H. Ahn, *Physical Review B*, 2012, **85**, 224404.
8. V. Bannikov, I. Shein, V. Kozhevnikov and A. Ivanovskii, *Journal of Structural Chemistry*, 2008, **49**, 781-787.
9. T. Gibb and M. Matsuo, *Journal of Solid State Chemistry*, 1990, **86**, 164-174.
10. A. M. Arévalo-López, F. Sher, J. Farnham, A. J. Watson and J. P. Attfield, *Chemistry of Materials*, 2013, **25**, 2346-2351.
11. F. Ramezanipour, J. E. Greedan, L. M. Cranswick, V. O. Garlea, J. Siewenie, G. King, A. Llobet and R. L. Donaberger, *Journal of Materials Chemistry*, 2012, **22**, 9522-9538.
12. F. Ramezanipour, J. E. Greedan, J. Siewenie, R. L. Donaberger, S. Turner and G. A. Botton, *Inorganic Chemistry*, 2012, **51**, 2638-2644.
13. E. Banks and M. Mizushima, *Journal of Applied Physics*, 1969, **40**, 1408-1409.
14. T. C. Gibb, *Journal of Materials Chemistry*, 1991, **1**, 23-28.
15. P. Battle, S. Bollen, T. Gibb and M. Matsuo, *Journal of Solid State Chemistry*, 1991, **90**, 42-46.
16. T. Gibb and M. Matsuo, *Journal of Solid State Chemistry*, 1990, **88**, 485-497.
17. R. Ravaud, G. Lemarquand and V. Lemarquand, *Tribology International*, 2010, **43**, 76-82.
18. H. Hartshorne, C. J. Backhouse and W. E. Lee, *Sensors and Actuators B: Chemical*, 2004, **99**, 592-600.
19. Z. Abbas, M. Surendran, P. A. Anjana, P.K.Jidev, H. Dasari, N. Sudhakar Naidu, S. Anandhan, K. U. Bhat, G. U. Bhaskar Babu and H. Prasad Dasari, *Materials Today: Proceedings*, 2017, **4**, 9360-9364.
20. J. Fransaer, J. Roos, L. Delaey, O. Van der Biest, O. Arkens and J.-P. Celis, *Journal of Applied Physics*, 1989, **65**, 3277-3279.
21. M. A. Zaitoun and C. Lin, *The Journal of Physical Chemistry B*, 1997, **101**, 1857-1860.
22. A. Varma, S. Deshpande and J. Kennedy, *Carbohydrate Polymers*, 2004, **55**, 77-93.
23. T. C. Gibb, *Journal of Materials Chemistry*, 1992, **2**, 57-64.
24. O. G. Rojas, G. Song and S. R. Hall, *CrystEngComm*, 2017, **19**, 5351-5355.
25. D. Lide, *Handbook of Chemistry and Physics*, 2000, 130-135.